Interannual Variations of Indian Summer Monsoon in a GCM: External Conditions versus Internal Feedbacks

B. N. GOSWAMI*

Program in Atmospheric and Oceanic Sciences, Princeton University, Princeton, New Jersey

(Manuscript received 8 September 1995, in final form 28 June 1997)

ABSTRACT

The potential predictability of the Indian summer monsoon due to slowly varying sea surface temperature (SST) forcing is examined. Factors responsible for limiting the predictability are also investigated. Three multiyear simulations with the R30 version of the Geophysical Fluid Dynamics Laboratory's climate model are carried out for this purpose. The mean monsoon simulated by this model is realistic including the mean summer precipitation over the Indian continent. The interannual variability of the large-scale component of the monsoon such as the ''monsoon shear index'' and its teleconnection with Pacific SST is well simulated by the model in a 15-yr integration with observed SST as boundary condition. On regional scales, the skill in simulating the interannual variability of precipitation over the Indian continent by the model is rather modest and its simultaneous correlation with eastern Pacific SST is negative but poor as observed. The poor predictability of precipitation over the Indian region in the model is related to the fact that contribution to the interannual variability over this region due to slow SST variations [El Niño–Southern Oscillation (ENSO) related] is comparable to those due to regional-scale fluctuations unrelated to ENSO SST. The physical mechanism through which ENSO SST tend to produce reduction in precipitation over the Indian continent is also elucidated.

A measure of internal variability of the model summer monsoon is obtained from a 20-yr integration of the same model with fixed annual cycle SST as boundary conditions but with predicted soil moisture and snow cover. A comparison of summer monsoon indexes between this run and the observed SST run shows that the internal oscillations can account for a large fraction of the simulated monsoon variability. The regional-scale oscillations in the observed SST run seems to arise from these internal oscillations. It is discovered that most of the interannual internal variability is due to an internal quasi-biennial oscillation (QBO) of the model atmosphere. Such a QBO is also found in the author's third 18-yr simulation in which fixed annual cycle of SST as well as soil moisture and snow cover are prescribed. This shows that the model QBO is not due to land-surface–atmosphere interaction. It is proposed that the model QBO arises due to an interaction between nonlinear intraseasonal oscillations and the annual cycle. Spatial structure of the QBO and its role in limiting the predictability of the Indian summer monsoon is discussed.

1. Introduction

The seasonal mean tropical circulation may be potentially more predictable than the middle latitude circulation as the low-frequency component of the tropical variability is primarily forced by slowly varying boundary conditions such as sea surface temperature (SST), soil moisture, etc. (Charney and Shukla 1981; Shukla 1981). This was supported by many studies with atmospheric general circulation models (GCMs) forced with observed SST (Lau 1985; Latif et al. 1990; Kitoh 1991; Goswami et al. 1995). Observational and modeling studies have established that the Indian summer monsoon is linked with several surface boundary forcings. In addition to links with Eurasian snow cover (Hahn and Shukla 1976; Dickson 1984; Vernekar et al. 1995) and soil moisture over the Indian continent (Shukla and Mintz 1982), the link with Pacific SST and the Southern Oscillation has been studied by many authors (Rasmusson and Carpenter 1983; Shukla and Paolino 1983; Yasunari 1991; Webster and Yang 1992). This background led to the optimism that long-range dynamical prediction of the Indian summer monsoon one or two seasons in advance may be feasible. As a result, a large number of studies in the last few years have made serious attempts to simulate the interannual variability (IAV) of the Indian summer monsoon (Palmer et al. 1992; Zwiers 1993; Chen and Yen 1994; Sperber and Palmer 1996) and to hindcast seasonal mean monsoon rainfall (Brankovic et al. 1994; Fennessy and Shukla 1994) using different atmospheric GCMs (AGCMs).

Most models can simulate the interannual variability of some planetary-scale component of the monsoon

* Current affiliation: Centre for Atmospheric Sciences, Indian Institute of Science, Bangalore, India.

Corresponding author address: Dr. B. N. Goswami, Centre for Atmospheric Sciences, Indian Institute of Science, Bangalore 560 012, India.
E-mail: goswamy@cas.iisc.ernet.in

such as the divergent circulation (as given by the velocity potential) or the ''monsoon shear index'' as defined by Webster and Yang (1992). However, the simulation of the IAV of the monsoon rainfall differs widely from one model to another (Sperber and Palmer 1996), indicating the great sensitivity of this regional part of the circulation on resolutions and physical parameterizations of the models. Another observation is that while the prediction of the seasonal mean rainfall in other parts of the Tropics (e.g., Sahel or equatorial Pacific) does not seem to be sensitive to small changes in the initial conditions, the simulation of the seasonal mean Indian monsoon rainfall seems to be rather sensitive to small changes in the initial conditions (Palmer and Anderson 1994; Brankovic and Palmer 1994). This indicates that the mean monsoon circulation in the Tropics may not be entirely forced by slowly varying boundary conditions but is also governed by internal dynamics to some extent. Some other models, on the other hand, do not show such sensitivity of the simulation of the mean monsoon on initial conditions (Fennessy and Shukla 1994). To obtain an estimate of the potential predictability of the Indian summer monsoon, we make quantitative estimate of contributions from boundary forcing and internal dynamics to the interannual variability of the monsoon in this study. Within the context of the model used, we also investigate the factors responsible for limiting the predictability.

Several recent studies (Harzallah and Sadourny 1995; Rowell et al. 1995; Stern and Miyakoda 1995; Dumenil et al. 1994) have made attempts to estimate the contribution of internal dynamics to low-frequency atmospheric variability in general. All these studies have utilized the ''analysis of variance'' technique with an ensemble of multiyear AGCM integrations with the same observed SST as boundary conditions. The forced variability may be defined as the ensemble mean, whereas the internal variability may be defined as the deviations from the ensemble mean. Harzallah and Sadourny (1995) used an ensemble of seven integrations with the Laboratoire de Meteorologie Dynamique GCM for 19 yr each with observed SST for 1970–88. D. Rowell (1996, personal communication) recently carried out an ensemble of six runs with the Hadley Centre model using observed SST for the recent 45 yr between 1948 and 1993 while Stern and Miyakoda (1995) have reported an ensemble of nine 10-yr integrations with the Geophysical Fluid Dynamics Laboratory (GFDL) dynamic extended range forecast model using observed SST for 1979–88. While Harzallah and Sadourny (1995) mainly explored the role of internal variability in the extratropics, Rowell et al. (1995) and Stern and Miyakoda (1995) presented the ratio of the internal variability to the forced variability over the Tropics too. They show that the spread among the ensemble (indicating sensitivity to initial conditions) is as large as the interannual variability itself. This indicates poor predictability of Indian monsoon rainfall. However, the precipitation climatology of both these models over the monsoon region during northern summer is not realistic. In both models, the ITCZ does not move over to the Indian continent during northern summer. Dumenil et al. (1994) carried out an ensemble of five integrations, each for 14 yr using observed SST for the period 1979–92 with their ECHAM3/T42 model. They also find a large spread in the simulation of the June–August (JJA) mean precipitation over the Indian region among the ensemble members, again indicating rather low predictability. The precipitation climatology during northern summer over the Indian region of this model too is much drier than observed. As the monsoon precipitation climatology of these models is not realistic, it may not be possible to make definitive conclusions regarding predictability of the monsoon based on these studies.

In the present study, we have adopted an alternative approach. First of all, as our primary objective relates to the predictability of the Indian summer monsoon, we select an atmospheric GCM whose precipitation climatology during the northern summer over the monsoon region is reasonably close to the observed climatology. Then, the forced variability is estimated from a multiyear integration of the model with observed SST. The internal variability is estimated from a multiyear run with the same model with climatological seasonal cycle SST. Another sensitivity experiment with the climatological seasonal cycle run has been conducted to derive some insight regarding the origin of the low-frequency oscillations in this run. The model used and the experiments conducted are described in section 2. The monsoon climatology of the model is discussed in some detail in section 3. The simulation of the SST forced interannual variations from the observed SST run are discussed in section 4. The physical mechanism through which the ENSO SST influence the monsoon rainfall is also examined in this section, using a multivariate empirical orthogonal function (MEOF) analysis. The interannual variability due to internal dynamics is examined in section 5. The amplitude of interannual variations of Indian summer monsoon indexes due to internal dynamics is compared to the amplitude of forced variability. The nature of the low-frequency variability in the climatological SST run is also investigated. It is discovered that the model atmosphere exhibits an internal quasi-biennial oscillation. Possible physical mechanisms for the origin of this biennial oscillation are also discussed in this section. A summary of the results is presented in section 6. The implications of our results to the predictability of Indian summer monsoon are discussed here.

2. The model and experiments

The atmospheric model used in this study is a version of the GFDL spectral climate model. This version has a rhomboidal 30 horizontal resolution (30 zonal waves and 30 associated Legendre functions; approximately

3.75° long × 2.25° lat resolution) and 14 unevenly spaced sigma levels in the vertical (R30L14 version). The sigma values corresponding to the 14 levels are 0.997, 0.979, 0.935, 0.866, 0.777, 0.676, 0.568, 0.460, 0.355, 0.257, 0.171, 0.101, 0.050, and 0.015. The vertical derivatives in the prognostic equations are computed by a centered, second-order finite-difference scheme. The lower-resolution version (R15L09) described by Gordon and Stern (1982) has been used in many climate studies (e.g., Delworth et al. 1993; Manabe and Stouffer 1994). The physical processes and their parameterizations included in this version of the model are briefly described in the appendix.

Three multiyear integrations are carried out with the model. The three experiments are briefly described below.

a. OBS-SST run

In this run the observed monthly mean global SST (Reynolds 1988) was prescribed. Monthly mean values were interpolated from one month to another month to produce the required daily values. The soil moisture and snow cover were predicted. The model was integrated for 15 yr with observed SST from January 1979 through December 1993. The model was initially spun up with climatological SST for 5 yr from a resting isothermal state.

b. CLI-SST run

In this run climatological seasonal cycle global SST was prescribed, which was repeated every year. The soil moisture and snow cover were predicted. This run was actually conducted much before the OBS-SST run was initiated. The climatological seasonal cycle of SST was taken from Levitus (1982). The climatological sea ice used in this run was taken from Walsh and Johnson (1979) and Zwally et al. (1983). The initial condition for this run consisted of a resting isothermal atmosphere. The model was integrated for 40 yr and the monthly mean values from the last 20 yr are considered here.

c. CSST-SM run

Both the seasonal cycle of SST and the seasonal cycles of soil moisture were prescribed in this run. The climatological SST used was same as in the CLI-SST run. The climatology of soil moisture at each grid point was constructed from the 15-yr simulations of the OBS-SST run. The snow cover feedback is also eliminated from the model by maintaining both snow depth and snowmelt zero everywhere. To account for the presence of snow cover, we replaced snow cover–dependent albedo computations with a prescribed distribution of the surface albedo, which is again obtained from the OBS-SST run. This integration was carried out for 18 yr. Monthly mean output is analyzed from all the runs.

3. Monsoon climatology of the model

The Asian summer monsoon has some unique characteristic features such as the low-level westerly jet over the north Arabian Sea and the easterly jet in the upper troposphere. The maximum strength of the easterly jet is at around 150 mb with its center shifted to the east of the low-level westerly jet center by about 10° long. In addition, the movement of the mean position of the ITCZ to the Indian continent and relatively sudden ''onset'' and ''retreat'' of the monsoon constitute other characteristic features of the Indian summer monsoon. In this section, we examine the GFDL R30L14 model's ability to simulate these features. As described in the previous section, we have three different multiyear simulations with the same model. Since the annual cycle of the SST is nearly identical and the annual cycle of the solar forcing is identical in all three experiments, the climatologies derived from the three runs are nearly identical. In Fig. 1, we show the precipitation climatology for January, August, and June–September (JJAS) mean from the OBS-SST run and compare them with observations (Legates and Willmott 1990). During winter, the position of the ITCZ is correctly simulated. However, the model simulates a smaller area of large precipitation (>8 mm day^{-1}) over Indonesia than observed. During summer, the ITCZ does move to a position over to the Indian continent. The maximum over the northern Bay of Bengal is well simulated. The precipitation over most of the Indian continent is reasonably well simulated. The maximum off the western coast is not well simulated. This is related to the model's resolution being insufficient to resolve the western Ghat mountains adequately. The seasonal mean (June–September) precipitation is also shown here, and as in our discussion of interannual variability we shall be referring to seasonal mean anomalies. It is noted that the seasonal mean precipitation is also well simulated by the model. The simulated precipitation over central India is slightly weaker than observed. However, the model simulated a much weaker secondary precipitation maximum around the equator during summer. Considering the low resolution of the model and the rather simple parameterization of cumulus convection employed by the model, the simulation of the precipitation climatology is realistic.

In Fig. 2, JJA mean vector winds at 860 mb and 170 mb derive from the OBS-SST run are shown. The simulated low-level jet is at the right place (around 12°N, 55°E) and of the right magnitude. However, the simulated southwesterlies penetrate a bit too far to the east (about 140°E), and the observed southwesterlies are not seen to go beyond 120°E. As 200 mb is not a standard level in our model, we show the winds at 170 mb, which happens to be close to the easterly jet maximum (150 mb). The jet maximum of about 35 m s^{-1} located around 70°E and between the equator and 10°N seems to be close to the observed location and strength of the jet maximum at 150 mb (Rao 1976). Thus, the strength and

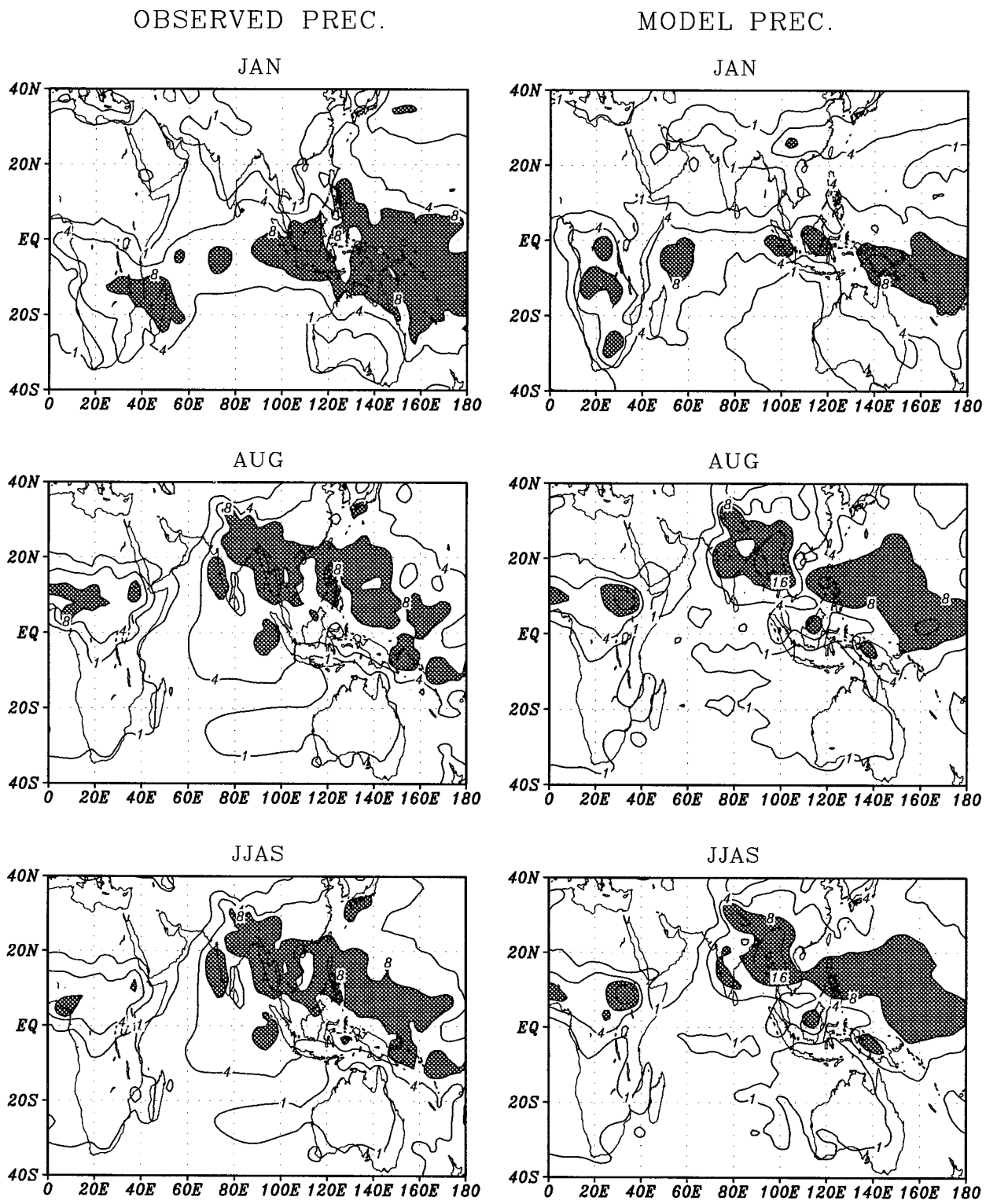

FIG. 1. Climatological mean January (Jan), August (Aug), and June–September (JJAS) precipitation. The mean derived from the OBS-SST run (right panels) is compared with observations (Legates and Willmott 1990, left panels). Contours are 1, 4, 8, 16, and 32 mm day^{-1}. Precipitation greater than 8 mm day^{-1} is stippled.

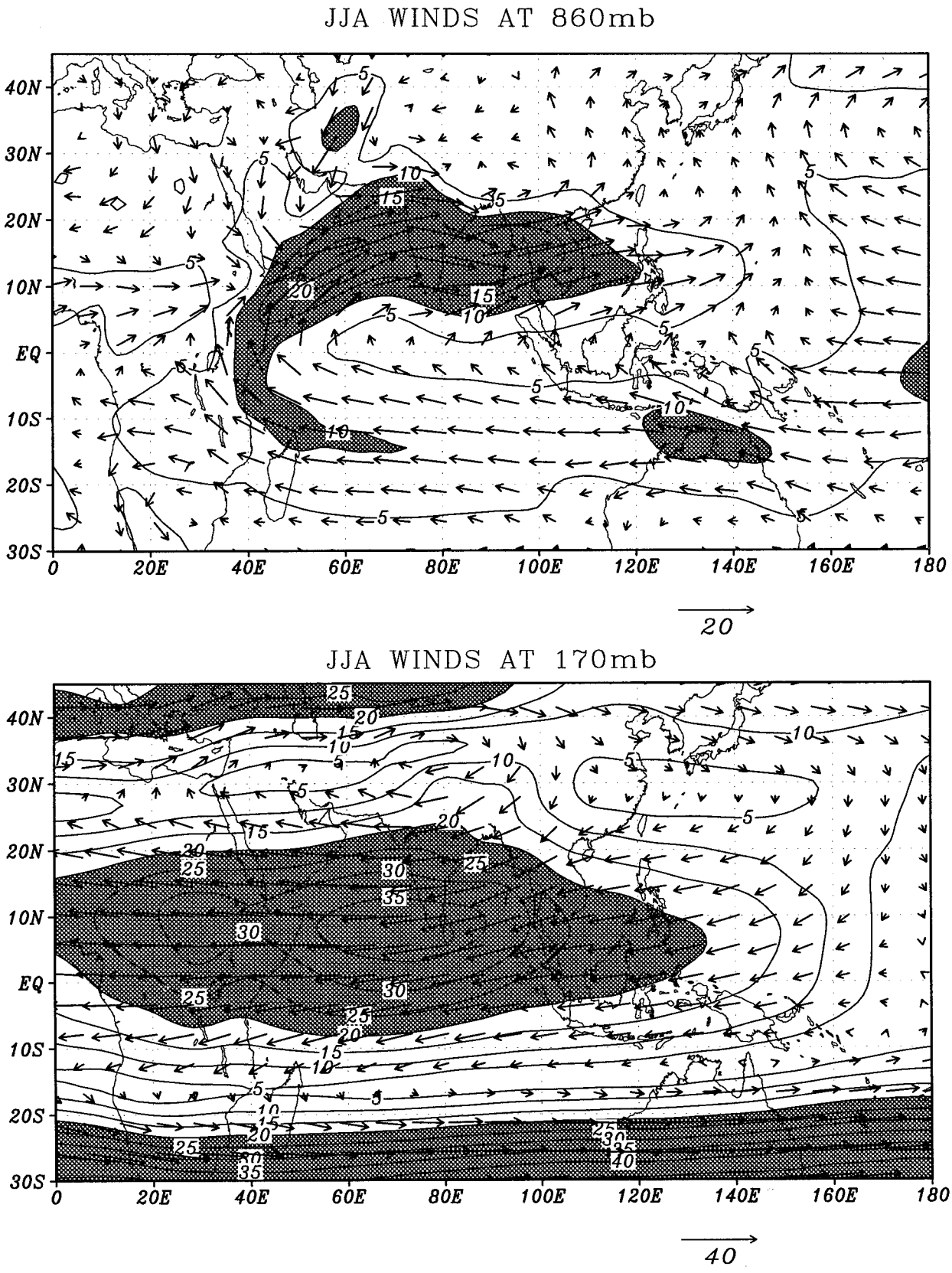

FIG. 2. Climatological mean June–August (JJA) averaged vector winds from the OBS-SST run at 860 mb and 170 mb are shown along with contours of the isolates. Contour interval in both cases is 5 m s^{-1}. Regions of winds stronger than 10 m s^{-1} at the lower level and 20 m s^{-1} at the upper level are stippled.

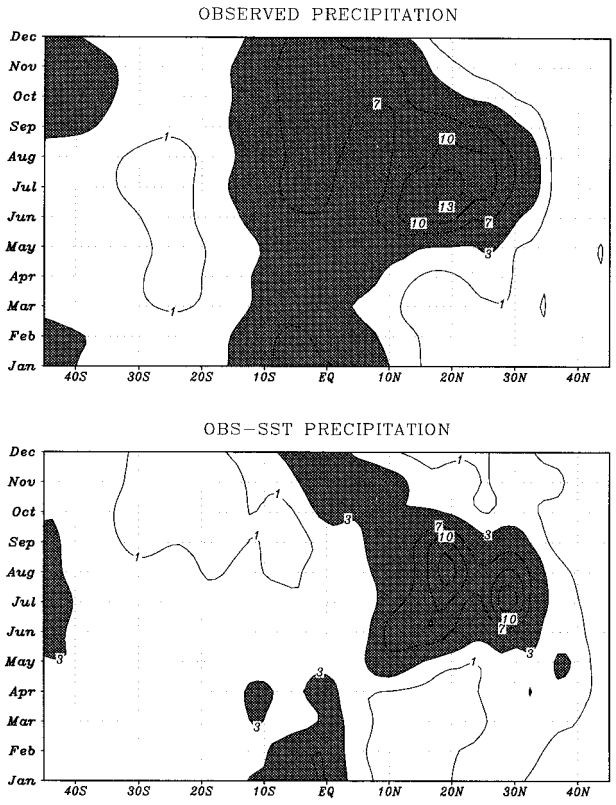

FIG. 3. Comparison of model-simulated onset and retreat of the monsoon with rainfall averaged between 70° and 95°E (lower panel) with observations (Legates and Willmott 1990). Precipitation greater than 3 mm day^{-1} is stippled.

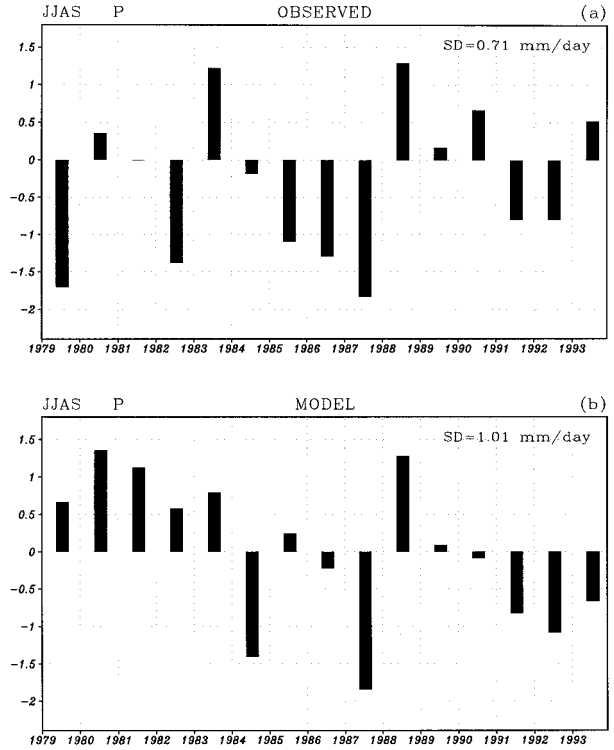

FIG. 4. Comparison of simulated interannual variability of the seasonal mean monsoon (June–Sept) precipitation with observations. (a) Observed ''all-India'' precipitation anomalies; (b) the simulated precipitation anomalies averaged over India and the Bay of Bengal (70°–95°E, 10°–30°N). In both cases the precipitation anomalies are normalized with their own standard deviation shown in each panel.

location of the simulated monsoon vortex seems to be reasonable.

In Fig. 3 we examine the onset and retreat of the monsoon. To illustrate this, we have plotted averaged precipitation between 70° and 95°E as a function of latitude and time of the year and compared it with observations. As in observations, we note that the onset of the simulated monsoon takes place rather rapidly in late May and retreats somewhat slowly in September–October. However, the simulated retreat is somewhat faster than observed. We note that the simulated averaged precipitation over the continent during the monsoon season is comparable to the observations. However, the model simulates too little rainfall over the equatorial Indian Ocean during the monsoon season. This systematic error may have some implications in the simulation of the intraseasonal monsoon oscillations (Goswami 1994).

4. Interannual variability: SST forced

a. Monsoon variability

In this section we discuss the interannual variability of some monsoon indices simulated by the model in the OBS-SST run. In Fig. 4, we examine the simulation of interannual variability of regional precipitation by the model. Here the seasonal mean (JJAS) precipitation anomalies averaged over the Indian region (70°–95°E and 10°–30°N including the oceanic region) are plotted and compared with observations. The amplitude of the interannual variability of precipitation over the Indian region simulated by the model (SD = 1.01 mm day^{-1}) is in fact slightly larger than the observed amplitudes (SD = 0.71 mm day^{-1}). The skill in simulating the interannual variability of the regional-scale precipitation by model is rather modest. It simulates the 1987 and 1988 dry and wet monsoons quite well. However, it fails to simulate the 1982 dry monsoon. Out of 15 yr, the sign of the precipitation anomaly is correctly simulated in 10 yr. The actual precipitation anomaly differences between 1983 and 1982 and 1988 and 1987 averaged for JJA are shown in Fig. 5. In both the ENSO cycles, the enhancement of the precipitation over Indonesia and the South China Sea during the cold phase and reduction in warm phase are well simulated. However, the anomalies over the Indian continent were not well simulated during 1982–83. The meridional dipole structure of the precipitation anomalies during 1988 and 1987 (Fig. 5b) is qualitatively similar to the meridionally dipolar heating diagnosed by Nigam (1994) although there are dif-

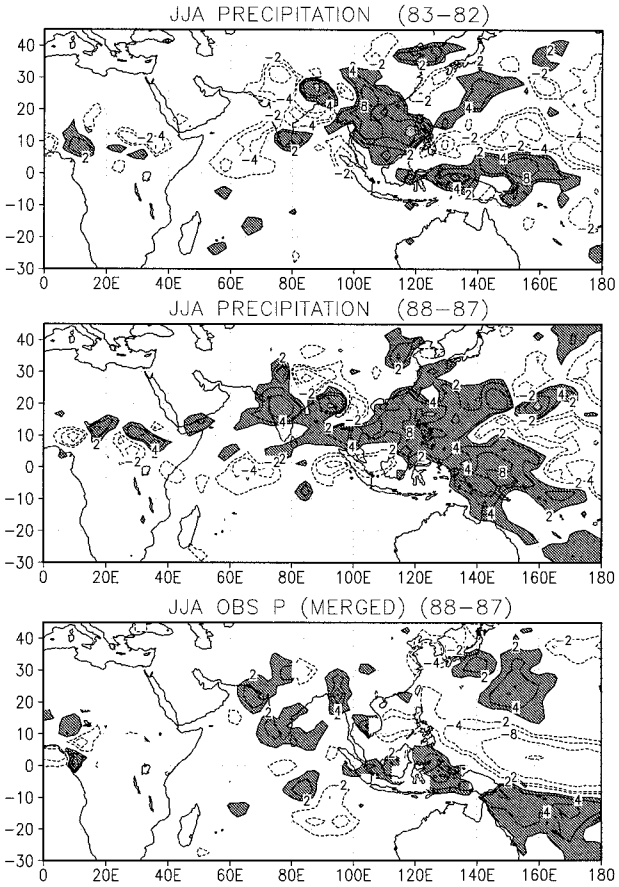

FIG. 5. Simulated JJA precipitation difference over the Asian monsoon region between consecutive La Niña and El Niño events, 1983 and 1982 (upper panel) and 1988 and 1987 (middle panel), respectively. Observed JJA precipitation difference between 1988 and 1987 based on merged data (gauge plus MSU) is shown in the lower panel. The contours are 2, 4, 8, and 16 mm day^{-1}. Positive anomalies greater than 4 mm day^{-1} are shaded. Negative contours are dashed.

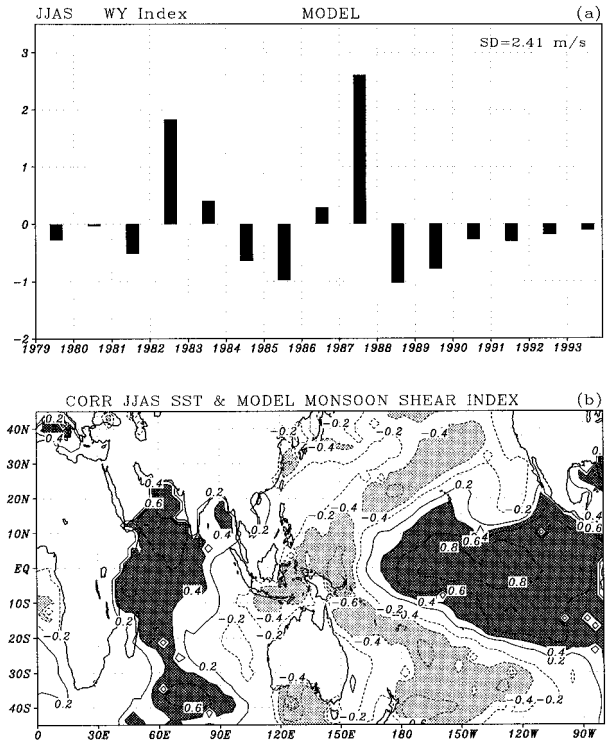

FIG. 6. Simulated monsoon shear index (zonal wind shear between 170 and 860 mb averaged over 40°–110°E, 0°–20°N) and its teleconnection with Indian and Pacific ocean summer SST. (Top) Interannual variability of the normalized shear index averaged over the summer (JJAS) and (bottom) correlation of the same with JJAS SST. Regions with positive correlation greater than 0.4 are shaded dark, and those with less than −0.4 are shaded light. The standard deviation of the shear index is shown in the top panel.

ferences in detail. In particular, the diagnosed equatorial band in his case is located between 5° and 10°N. This difference may be partly due to differences in the systematic biases in the two models. In Fig. 5c, we show JJA precipitation anomaly difference between 1988 and 1987 based on merged precipitation prepared by J. K. E. Schemm and based on station data over land and oceanic precipitation from microwave sounding unit (MSU) measurements. It is seen that MSU precipitation does show a tendency for decreased precipitation over the equatorial region during the summer of 1988 compared to that of 1987.

Next, we examine the simulation of interannual variability of one large-scale index of the monsoon as defined by Webster and Yang (1992). In the context of our model, we define this index as vertical zonal wind shear (170–860 mb) averaged between 40° and 110°E, and 0° and 20°N. The interannual variability of the simulated JJAS averaged monsoon shear index and its teleconnection with JJAS SST are shown in Fig. 6. It is clear that the simulated monsoon shear index reproduces the observed teleconnection pattern quite well (see Fig. 7b of Sperber and Palmer 1996). Thus, the simulation of the large-scale response to ENSO SST variations by the model is realistic.

The limited ability of the GCM to simulate the observed interannual variability of precipitation over the Indian region is characteristic of most GCMs (Sperber and Palmer 1996). The simultaneous correlation between observed summer precipitation over India and the eastern Pacific SST is negative and only about −0.4 (Yasunari 1991). The correlation of JJAS simulated precipitation over India and the eastern Pacific SST is also weakly negative (−0.3). Within the context of the present model we investigate how ENSO-SST tends to induce reduction in monsoon precipitation and why the relationship is weak.

b. ENSO–monsoon connection

Several studies have attempted (Webster and Yang 1992; Nigam 1994) to identify the physical mechanism through which ENSO-related SST anomalies influence the precipitation over the Indian monsoon region. It has

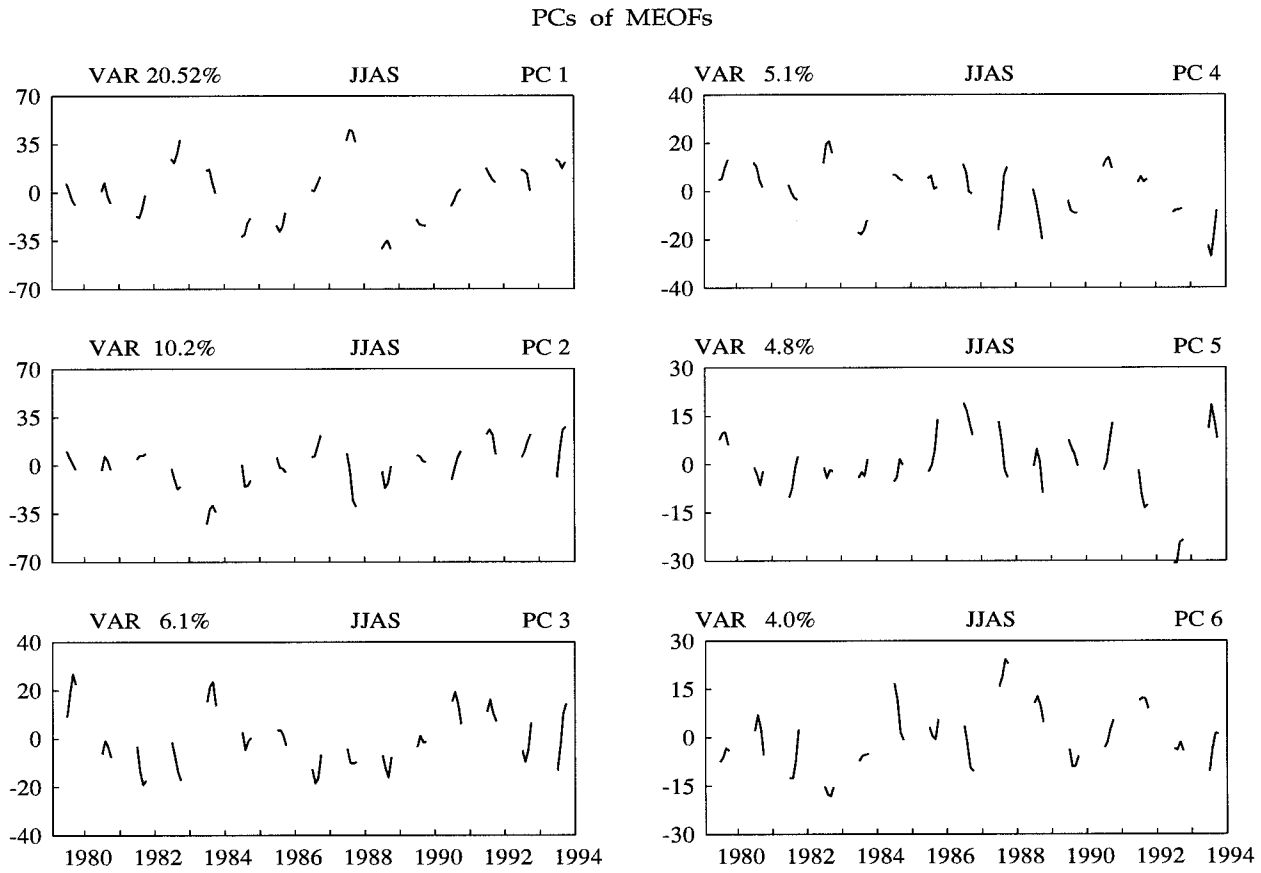

FIG. 7. Time series of the first six principal components of the MEOF analysis. As only June–September months are used, the time series is broken in between. Percentage of total variance explained by each EOF is also shown. Units are arbitrary.

been postulated that the movement of the ascending branch of the Walker circulation to the eastern Pacific during warm episodes is somehow responsible for the reduction of precipitation over the Indian continent. Nigam (1994) diagnosed the diabetic heating over the Indian region during JJA of 1987 and 1988 as a residual in the thermodynamic equations from uninitialized but mass-balanced European Centre for Medium-Range Weather Forecasts analysis. Using a linear primitive equation steady-state model he showed that the circulation changes during the El Niño (1987) and La Niña (1988) years over the Indian region are consistent with the meridionally dipolar heating anomalies during these years. Nigam (1994) found that for JJA (1987–88) monsoon anomaly, the interaction between zonally symmetric circulation and Himalayan–Tibetan orography explained a large part of the low-level divergence over Indochina. No study, however, has clearly established how the circulation changes associated with the shift of the Walker cell result in a reduction of the continental precipitation over India. This is partly due to the fact that monsoon is not only affected by the large-scale circulation associated with ENSO but is also affected by regional-scale circulations. Unless one is able to separate the ENSO response from the other regional-scale effects, it is not possible to elucidate how ENSO affects the monsoon. Here, we use a different technique to achieve this. We use an MEOF analysis employing singular value decomposition technique (Nigam and Shen 1993; Wang 1992) to bring out the structures related to different modes of variability. This method provides an efficient way of compacting a large volume of multifield data and allows us to isolate dominant modes of variability from the noise. As the geophysical fields are not only correlated spatially but are also correlated among themselves, this technique helps us bring out the three-

→

FIG. 8. Spatial distribution of the loadings of the first EOF. Units are arbitrary. Positive contours are solid and negative contours are dashed lines. (a) SST, contour interval = 0.5×10^{-2}; (b) precipitation, contour interval = 1.0×10^{-2}; (c) surface pressure, contour interval = 0.5×10^{-2}; (d) divergence at 860 mb, contour interval = 1.0×10^{-8}; and (e) vertical zonal wind shear between 170 and 860 mb, $U_{170} - U_{860}$, contour interval = 2.0×10^{-2}.

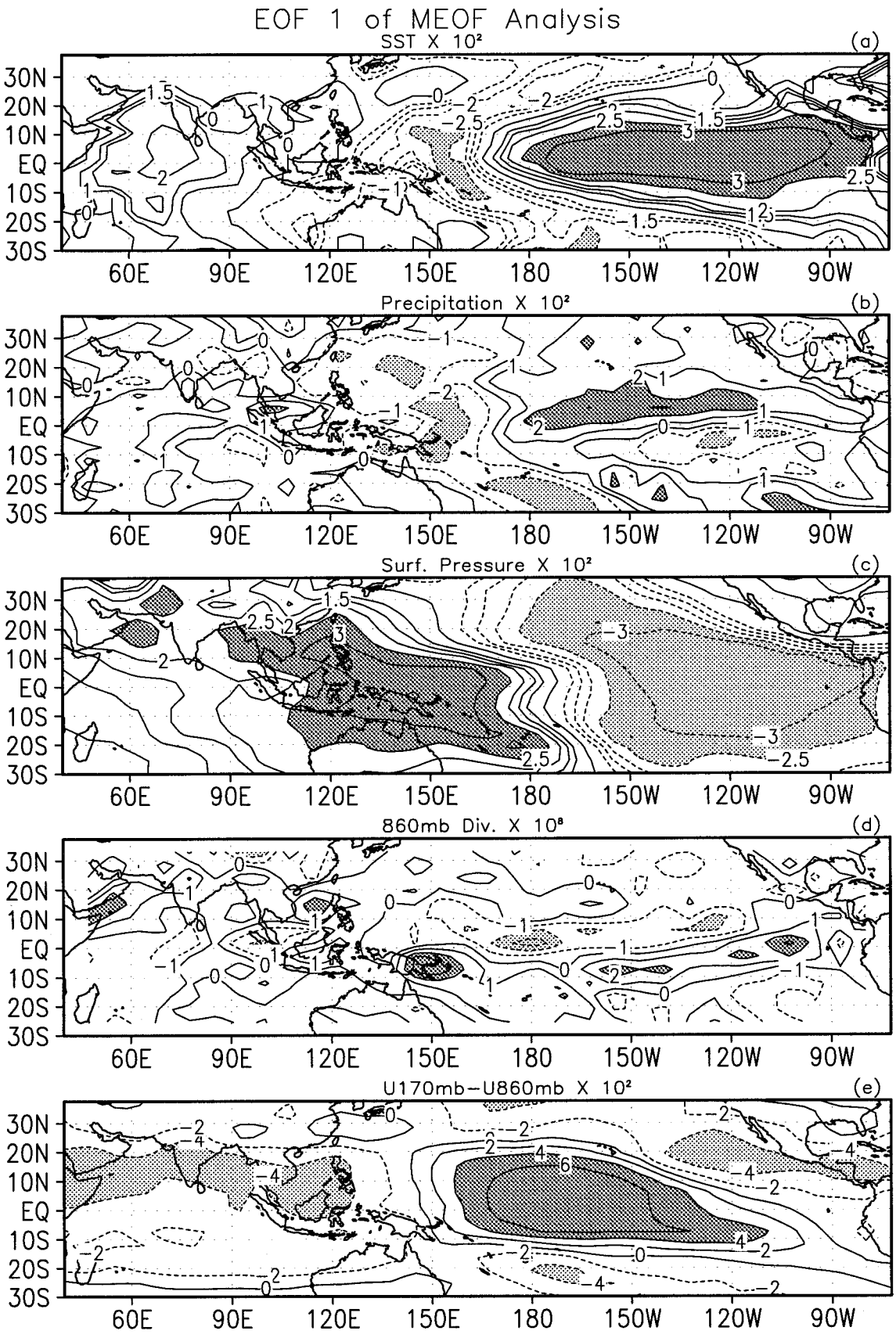

dimensional structure of anomalies associated with certain modes of variability lending insight into the dynamics of this variability.

We use SST, precipitation, surface pressure, zonal, and meridional components of wind at 860 mb and the zonal wind at 170 mb simulated in the OBS-SST run. As we are basically interested in the pattern of variability only during the summer season, anomalies for only June, July, August, and September for all years are used. The domain of analysis is taken from 20°E to 70°W and 35°S to 35°N. All the variables are normalized using their individual variance (Nigam and Shen 1993) before conducting the MEOF analysis. The first six EOFs explain 20.5%, 10.2%, 6.1%, 5.1%, 4.8%, and 4.0% of the total variance, respectively, and seem to be above the noise level (North et al. 1982). The time series of the amplitudes of the first six EOFs (principal components, PC) are shown in Fig. 7. The units of the principal components are arbitrary. The product of these amplitudes with the loadings for the EOFs and the corresponding variance for the individual fields would give an idea of the anomaly fields associated with these EOFs. The spatial patterns of the first, second, and the third EOFs are shown in Figs. 8–10. Instead of plotting all the fields, we plotted SST, precipitation, surface pressure, and two derived fields. We plot the divergence field calculated from the EOF patterns of the winds at 860 mb. This has been done to derive insight into the maintenance of the precipitation patterns associated with these EOFs. As the shear of the winds between the upper and lower atmosphere is a measure of the strength of the baroclinic circulations associated with tropical heating (Webster and Yang 1992), we also plot the shear between the zonal wind at 170 and 860 mb.

The first EOF (Fig. 8) and the second EOF (Fig. 9) clearly represent the model's response to SST variations associated with ENSO. Figure 7 shows that the first and second principal components have a dominant periodicity with period between 4 and 5 yr. The SST patterns for EOF1 (Fig. 8) and EOF2 (Fig. 9) also correspond closely to the SST anomaly patterns associated with ENSO. The precipitation patterns in both these two EOFs are closely related to the corresponding SST patterns. The phase difference between the low-frequency peaks of the first and second principal components together with the eastward displacement of the EOF2 SST pattern relative to that of EOF1 represent an eastward migration of the anomalies during the evolution of a warm event as observed during 1982–83. Thus, the EOF2, in some ways represents the abnormal conditions during the 1982–83 warm event. The precipitation field for EOF1 shows clearly increased precipitation over the central and eastern Pacific, decreased precipitation over the western Pacific, and increased precipitation over the central and eastern equatorial Indian Ocean. The negative pattern over the western Pacific extends northwestward but barely reaches the Indian subcontinent. The surface pressure pattern bears a resemblance to the classic Southern Oscillation pattern. The divergence field at 860 mb shows that the precipitation pattern is directly related to the low-level convergence/divergence. The increase in precipitation over the equatorial Indian Ocean is due to an increase in low-level convergence. The increase in the low-level convergence in the equatorial Indian Ocean in turn is related to large-scale circulation changes shown by the shear field. Associated with the movement of the Walker circulation, a strong anomalous low-level divergent circulation is set up in the western Pacific around 150°E. The low-level winds from this region converge to the equatorial Indian Ocean leading to the small increase of the low-level convergence there.

Consistent with the above picture, we now describe how warm phases of ENSO tend to be related to a decrease in precipitation over India. The summer monsoon precipitation over India results from the movement of the ITCZ to a northerly position at about 25°N. However, the ITCZ does not sit there throughout the whole season. Associated with the intraseasonal oscillations of the monsoon, the ITCZ keeps moving back and forth between this position over the continent and another favorable position over the equatorial Indian Ocean (Sikka and Gadgil 1980; Gadgil 1988). The favorable position of the ITCZ over the land is related to the land heating and the formation of the quasi-stationary monsoon trough, and the favorable position over the ocean is related to the existence of warm waters with temperatures greater than 28°C there (Goswami et al. 1984). Averaged over the whole summer season, the ITCZ spends more time over land than over the ocean leading to more rainfall over land in a normal year than over the ocean (Fig. 1). One possible reason why the land position occurs more often than the oceanic one is that the large-scale subsidence from the descending branch of the Walker circulation provides an inhibiting factor for formation of deep convection over the equatorial warm waters in the Indian Ocean. During the warm phases of ENSO, the movement of the ascending branch of the Walker circulation to the eastern Pacific removes the large-scale inhibiting factor and results in an enhanced low-level convergence over the warm equatorial waters. These large-scale circulations during the warm phases of ENSO allow the equatorial ITCZ to form more frequently and for longer periods. This leads to enhanced precipitation over the ocean and in turn produces subsidence over the land through the local Hadley circulation, resulting in decreased precipitation over the continent as seen from EOF1.

It is clear from Fig. 7 that while the first two PCs are associated with low-frequency oscillations (≈4–5 yr) associated with the ENSO period, the next four PCs are associated with a considerable amount of higher-frequency oscillations. The spatial pattern of the loadings for the third EOF is shown in Fig. 10. It is seen that these EOFs have spatial scales smaller than those associated with EOF1 and EOF2. If we look at the tem-

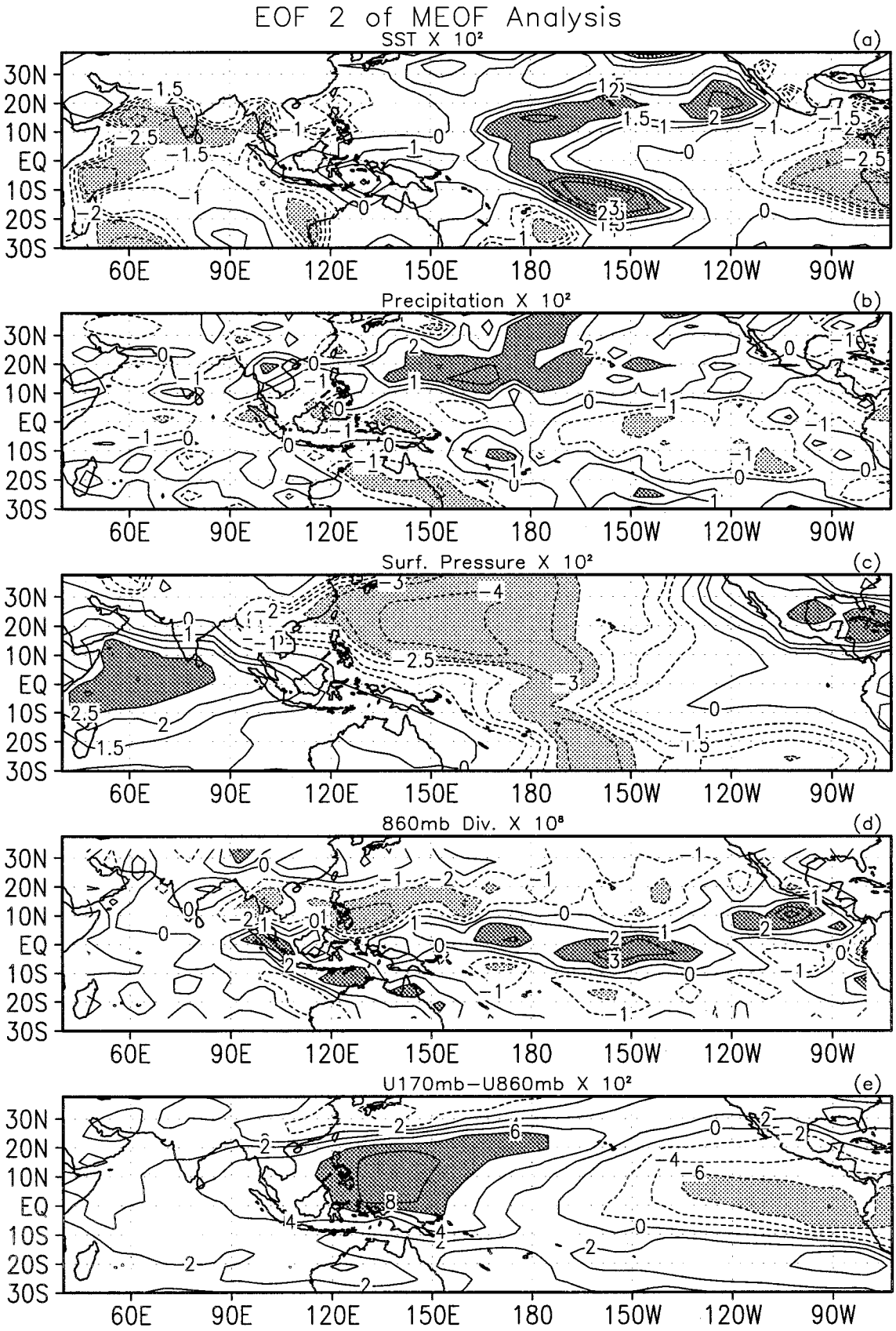

FIG. 9. Same as Fig. 8 but for the second EOF.

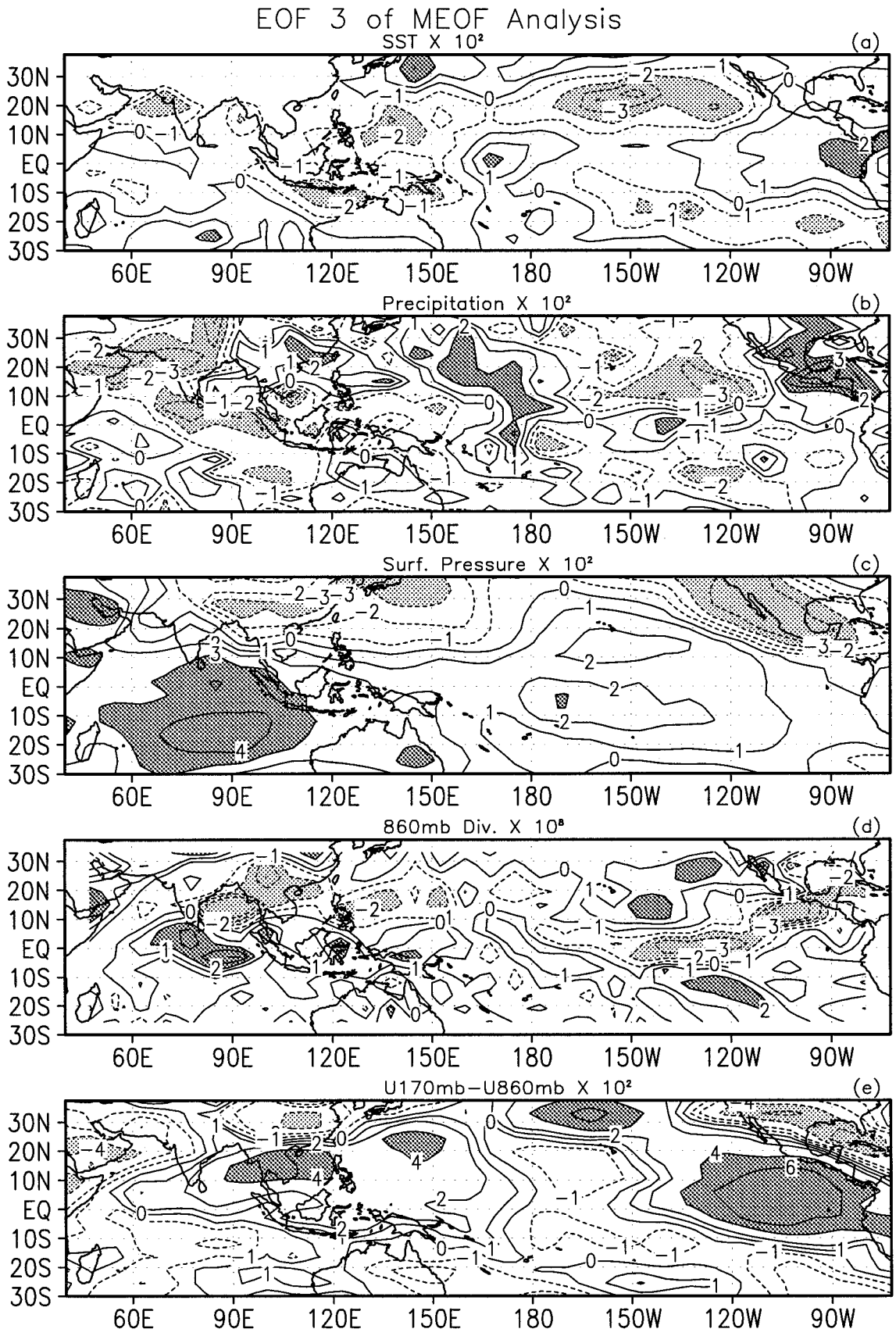

FIG. 10. Same as Fig. 9 but for EOF3; contour intervals are 1 in panels (a)–(d) and 2 in panel (e).

poral variations of EOF3 (i.e., PC3), it may appear that it also has a low-frequency component and should be associated with EOF1 and EOF2. However, it is rather intriguing that EOF3 does not have significant SST loading over Indonesia and the western Pacific where most of the precipitation anomaly takes place. The precipitation pattern associated with this EOF may be due to some internal oscillation of the organized convection over the warm pool in this region. Thus, it appears that EOF3 (and maybe the other higher EOFs) is not directly forced by SST variations. Similar to EOF3, EOF4, EOF5, and EOF6 also have (not shown) large loadings over the Indian and Indonesian region. Thus, the first two EOFs represent planetary-scale variability associated with the ENSO and the third through sixth EOFs represent some regional-scale variability due to various as yet unidentified causes.

The first and the second EOFs explain the largest and next largest amount of spatially averaged variance, but they both have very weak loadings over the Indian region. This means that the anomalies associated with these two modes over the Indian region are much smaller than those over the Pacific. EOF3–EOF6 all have much higher loadings over the Indian region. Therefore, it is possible that the anomalies associated with the regional-scale modes (EOF3–EOF6) may be comparable to the anomalies associated with the planetary-scale modes (EOF1–EOF2) over the Indian region. To establish this convincingly, we carried out a rotated principal component analysis of the same EOFs following Nigam and Shen (1993). Based on the rotated EOFs and their principal components, contributions to precipitation anomaly were calculated. In Fig. 11, the contributions to the precipitation anomaly from the planetary-scale modes (REOF1 and REOF2) and regional-scale modes (REOF3–REOF6) are shown over the continental region (70°–95°E, 10°–30°N) and equatorial Indian Ocean (70°–95°E, 5°S–5°N), respectively. The main point to note is that over the monsoon region, the contribution of the regional-scale modes is comparable to that from the planetary-scale modes. Over the equatorial region, however, the planetary-scale modes contribute significantly to the precipitation anomaly. The other important point to note is that the precipitation anomalies associated with the planetary-scale modes over the monsoon continent is always out of phase with that over the equatorial Indian Ocean.

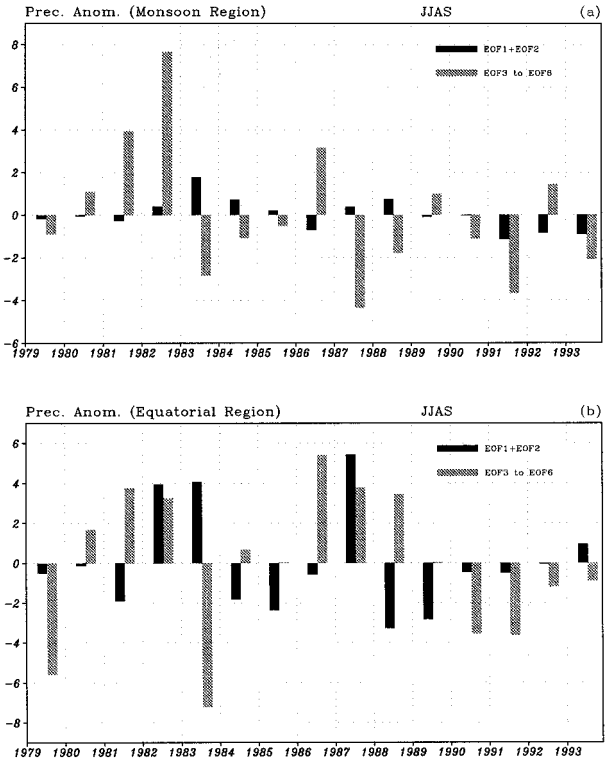

FIG. 11. Precipitation anomalies (mm day^{-1}) during the summer monsoon season (JJAS) over (a) continental monsoon region, 10°–30°N, 70°–95°E and (b) equatorial region, 5°S–5°N, 70°–95°E. Contribution from EOF1 and EOF2 is shown by dark bars and contribution from EOF3–EOF6 is shown by light bars.

5. Interannual variability: Internally generated

a. Monsoon variability in the CLI-SST run

To estimate how much of the interannual variability of the monsoon discussed in the previous sections is due to SST forcing and how much may be due to internal dynamics, we compare the interannual variability among the OBS-SST and CLI-SST runs. Figure 12 shows the precipitation averaged over the Indian monsoon region and the monsoon shear index as defined in section 4 from the CLI-SST run. Both indexes are averaged over the summer monsoon season, June–September. An examination of the interannual variability of the precipitation index shows that, although the observed SST (Fig. 4b) tends to enhance the variability (SD = 1.01 mm day^{-1}), the internal dynamics produce considerable variability (SD = 0.82 mm day^{-1}). The simulation of the monsoon shear index also show that the amplitude of the interannual variability generated purely by internal dynamics (Fig. 12b, SD = 1.92 m s^{-1}) is comparable to that forced by the slowly varying SST boundary forcing (Fig. 6a, SD = 2.41 m s^{-1}). In the OBS-SST run the entire variability is dominated by the 1987 event. The interannual variability produced by the internal dynamics is often larger than that in the SST boundary forced run. From the comparison of the standard deviations we can conclude that about 60% of the observed interannual variance of the monsoon may be accounted for by the internal dynamics.

b. Potential predictability of summer (JJA) precipitation

As is clear from the above discussion, the enhancement of potential predictability of the Indian summer

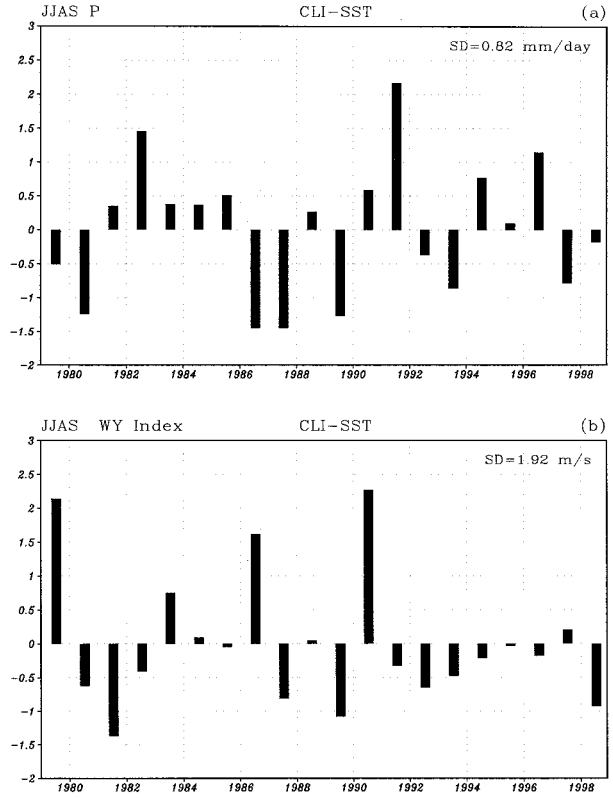

FIG. 12. Normalized interannual variation of two summer monsoon indexes from CLI-SST runs. (a) Seasonal mean (JJAS) precipitation averaged over the Indian region (70°–95°E, 10°–30°N), (b) monsoon shear index as defined in Fig. 6 (WY Index). The SD of each index is also shown. The CLI-SST run is for 20 yr and the year labeling is arbitrary here. To match with Fig. 4 and Fig. 6, the starting year is taken as 1979.

monsoon by ENSO SST variations is rather modest. There may be other regions in the Tropics where the summer precipitation may be potentially more predictable. To explore this, we plot in Fig. 13, the variance of JJA precipitation in the OBS-SST run over the whole tropical belt (50°S–50°N). We also plot the ratio of variances of JJA precipitation between the OBS-SST run and CLI-SST run. To avoid large ratios arising purely due to numerical errors in trying to calculate the ratio between two very small numbers, we have avoided calculation of the ratio when the variance of the number is less than 0.1 $(\text{mm day}^{-1})^2$. As the variance for the OBS-SST run is based on 15-yr data while that of the CLI-SST run is based on 20-yr data, the ratio must be greater than 2.65 (obtained from F table with 14 and 19 degrees of freedom) to reject the null hypothesis that the variance in the OBS-SST run is indistinguishable from the internal variability in the CLI-SST run with 97.5% confidence. It is seen that a clear signal of enhanced predictability is seen only over the equatorial eastern Pacific. There is also some enhancement of predictability in the eastern Atlantic. Some enhancement of predictability is also seen over northern Australia and the southeastern equatorial Indian Ocean. Averaged over the Indian monsoon region, the enhancement of predictability is not significant (consistent with Fig. 12) as there are only two small regions where the ratio is significant.

c. A quasi-biennial internal oscillation

From the above discussions, it is clear that the model atmosphere can generate significant interannual variability even in the absence of any external forcing with interannual periods. One important question that arises is, what then is responsible for these interannual variations? Are there significant natural oscillations of the system or are they simply part of a red-noise process? To derive some insight into these questions, we further investigate the nature of the low-frequency variability in the CLI-SST run. The 5-month running means of three different variables averaged over three different regions from the CLI-SST run are shown in Fig. 14. The precipitation over 5°S–5°N and 140°–160°E. The zonal winds at 170 mb and 860 mb are averaged over 5°S–5°N and 140°–180°E and 50°–70°E, respectively. The averaging regions for the winds are selected either to the east or to the west of the precipitating region with the assumption that the precipitation variations may be responsible for generating the wind anomalies. It is clear that all the three variables show significant low-frequency variability. In particular the precipitation time series tends to indicate a quasi-biennial variability. Quasi-biennial variations can also be detected in the wind time series. This preliminary examination indicates that the model atmosphere may have a quasi-biennial internal oscillation.

To establish whether there exists a significant quasi-biennial component in the CLI-SST run we carried out a spectrum analysis of the monthly mean time series shown in Fig. 14. The monthly means are used without additional filtering so that we avoid any bias that may be introduced due to the running mean calculations and so we could calculate the significance limits using lag 1 autocorrelations of the original time series. The spectra and the 95% confidence limits are shown in Fig. 15. It is noteworthy that all three time series have statistically significant peak with about a biennial periodicity. We must add here that the three regions shown here have been selected after some trial and error. As we shall show shortly, the biennial variability has some regional-scale structure. Therefore, if we average the anomalies over some arbitrary regions, there is a danger of canceling positive and negative anomalies leading to an insignificant signal. This is similar to the findings of Ropelewski et al. (1992), who found that the observed tropospheric biennial signal in surface winds and SST too is not significant at all locations.

Having established that there exists a significant quasi-biennial internal oscillation of the model atmosphere at some locations, we examined the spatial distribution of this mode. The biennial signal is first filtered from model

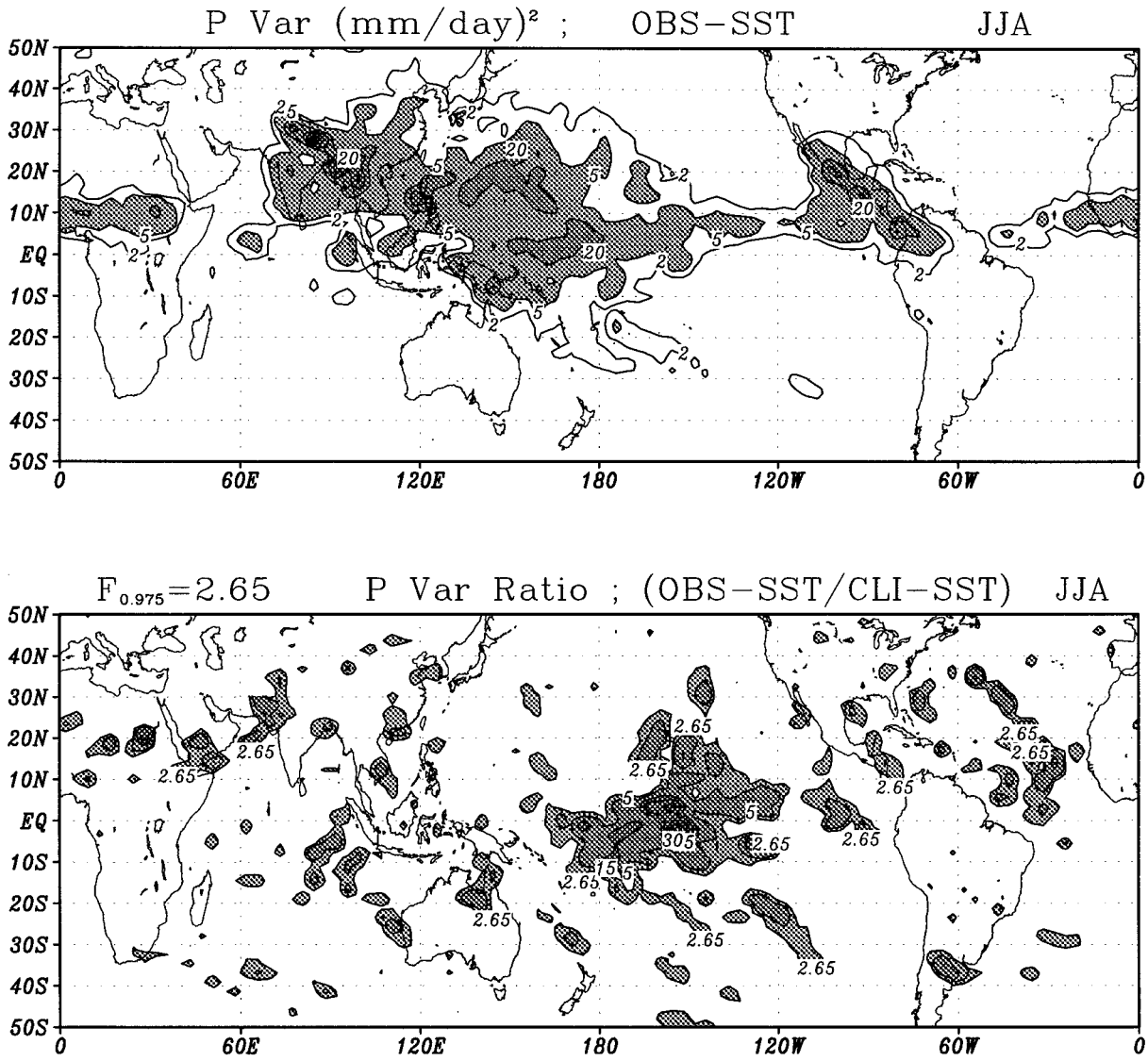

FIG. 13. Potential predictability of Northern Hemispheric summer (JJA) precipitation. (a) Variance of JJA precipitation from OBS-SST run. Contours 2, 5, 20, 35, 50, 65, and 80 (mm day^{-1})^2; (b) ratio of variances of JJA precipitation between OBS-SST run and CLI-SST run. Contours of the ratio larger than F value or 97.5% significance level (2.65) are only plotted. Contour levels are 2.65, 5, 15, 30, 50, 65, and 80.

precipitation and zonal winds at 860 and 170 mb using a Butterworth filter with peak response around 24 months and half-responses at around 18 and 32 months, respectively. The standard deviation of the biennial signal is then calculated at each grid point and compared with the standard deviation of the full field. We note that the total precipitation field has the highest variance over the Indian monsoon region, the Indonesian warm pool region, and over the Central American monsoon regions (Fig. 13a). The biennial filtered precipitation also has largest variance over more or less the same regions (not shown). It is noted that the internal biennial mode (CLI-SST run) explains as much of the total zonal wind variance (6%–12%) at 860 mb as does the forced biennial mode (OBS-SST run). The important question then is what causes the fluctuation of the precipitation and the winds at this timescale without any external forcing?

d. Possible mechanisms

Air–sea coupling, air–land surface coupling (Meehl 1987, 1993, 1994), and interaction between nonlinear intraseasonal oscillations and the annual cycle (Goswami 1995) have been invoked to explain the origin of the observed biennial component of the interannual variability in the Indian and Pacific region. As climatological SST is prescribed in our run, ocean–atmosphere coupling could not be responsible for our biennial oscillation. The other possibility is the atmosphere and land surface feedback as envisaged by Meehl (1994).

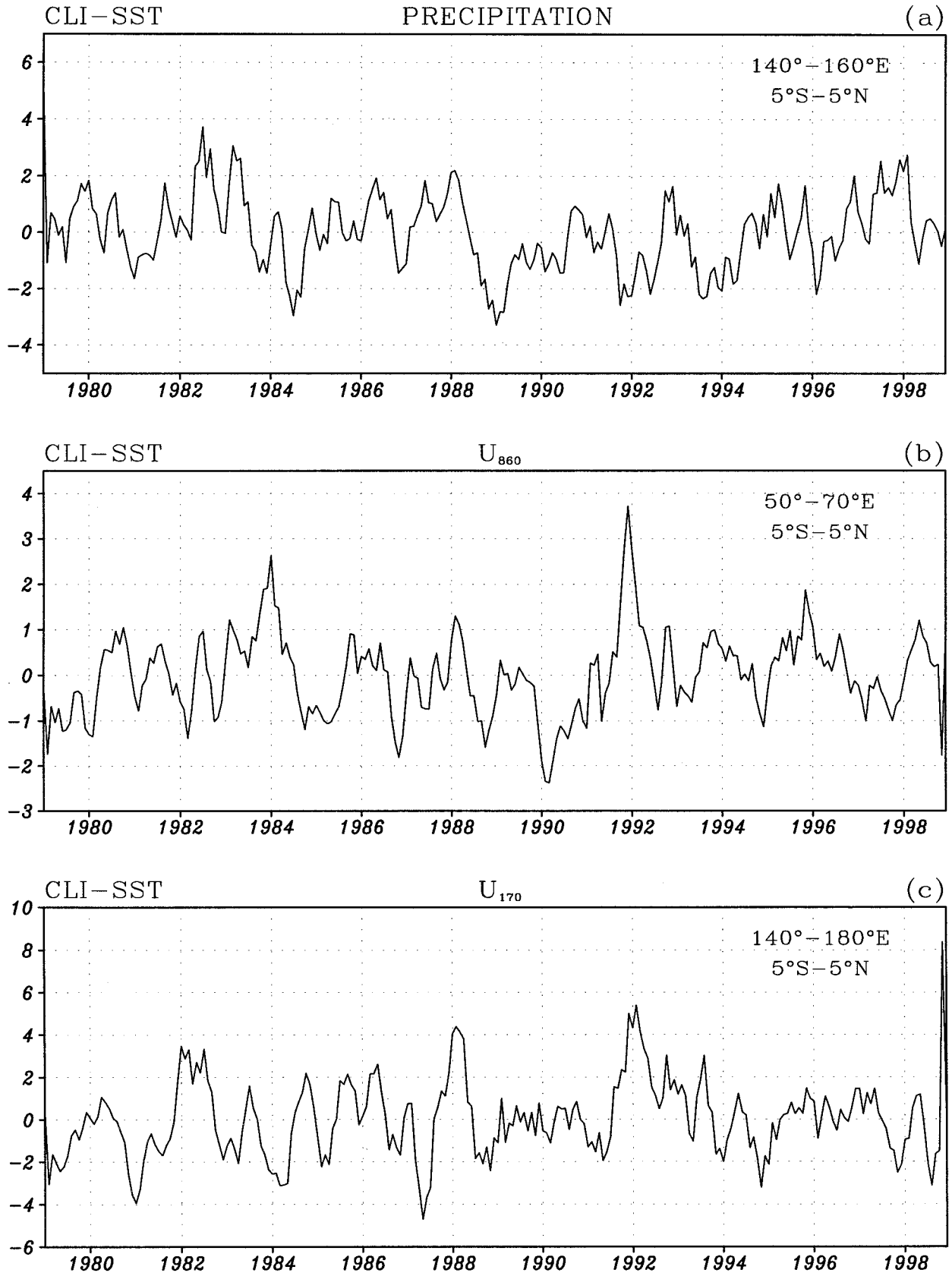

FIG. 14. The interannual variability in the CLI-SST simulation. Time series of 5-month running mean equatorial (5°S–5°N) precipitation P (mm day^{-1}, 140°–160°E) and zonal wind at 170 mb (140°–180°E) and 860 mb (50°–70°E) (m s^{-1}).

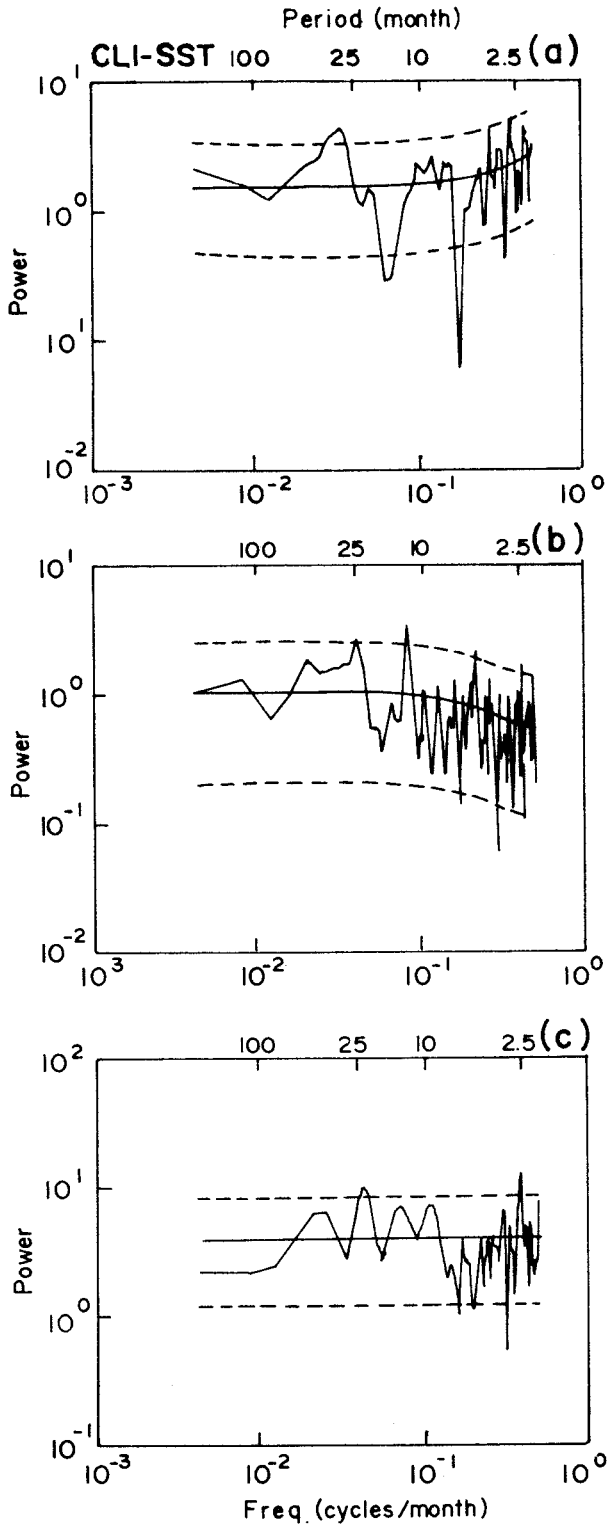

FIG. 15. Power spectra of unfiltered monthly precipitation and zonal winds averaged over the same regions shown in Fig. 12, for the CLI-SST run. (a) Precipitation (5°S–5°N, 140°–160°E), (b) zonal wind at 860 mb (5°S–5°N, 50°–70°E), (c) zonal wind at 170 mb (5°S–5°N, 140°–180°E). The theoretical red-noise spectrum based on lag 1 autocorrelations (thick sold) and the 95% confidence limit (broken line) are also shown.

Qualitatively, this feedback may be described as follows. The strength of the monsoon circulation is related to the north–south temperature gradient over the region. A strong monsoon is associated with a strong north–south temperature gradient and results in excess precipitation and soil moisture over land. If (and this is a big if!) the enhanced soil moisture persists through the next three seasons, land would be wetter than normal prior to the next monsoon. Evaporation and enhanced latent heat flux would result in cooler land temperature and weaker north–south temperature gradient, leading to a weaker monsoon. A weak monsoon this year would be associated with below-normal precipitation, which through the same arguments presented above would lead to strong north–south temperature gradient and a strong monsoon next year. In this manner the cycle could be repeated every 2 yr. While this mechanism could work in principle, there is no convincing evidence that soil moisture anomalies persist for three or more seasons. To determine whether this feedback is at work in producing the biennial oscillation in our model atmosphere, we carried out an additional multiyear run in which the annual cycle of the soil moisture and snow cover were prescribed (CSST-SM). The experiment was conducted for 18 yr. We then carried out time series and spectrum analysis of various monthly mean fields as before. It is found that this experiment also simulates a significant biennial signal as a dominant part of its interannual variability. The spectra of unfiltered monthly mean precipitation averaged over two locations are shown in Fig. 16. It is clear that both the time series show a rather strong and significant peak with a period around 2 yr. Therefore, it appears that the biennial oscillation of our model atmosphere does not owe its origin to a ground hydrology feedback as envisaged by Meehl (1994). With the external forcing associated with SST and ground hydrology feedback both being ruled out as a possible mechanism, it is clear that the biennial oscillation of the model atmosphere is due to some internal feedback. The only internal feedback one can think of at the present time is the one proposed by Goswami (1995). He showed that modulation energetic intraseasonal oscillations by the annual cycle could give rise to a quasi-biennial oscillation. The fact that an earlier version with very weak intraseasonal oscillations could not simulate a biennial mode in the climatological SST run (Alexender and Weikman 1995) while the present version with energetic intraseasonal oscillations (Hayashi and Golder 1993) could simulate the biennial oscillation indirectly supports our hypothesis. However, this is still a hypothesis and needs to be supported with additional experiments. It may be recalled that the present model ignores the role of vegetation in calculating soil moisture. Therefore, the role of ground hydrology feedback on the origin of the observed tropospheric QBO may still not be ruled out.

As the main objective of this study has been to quantify the contributions of the internal oscillations in the

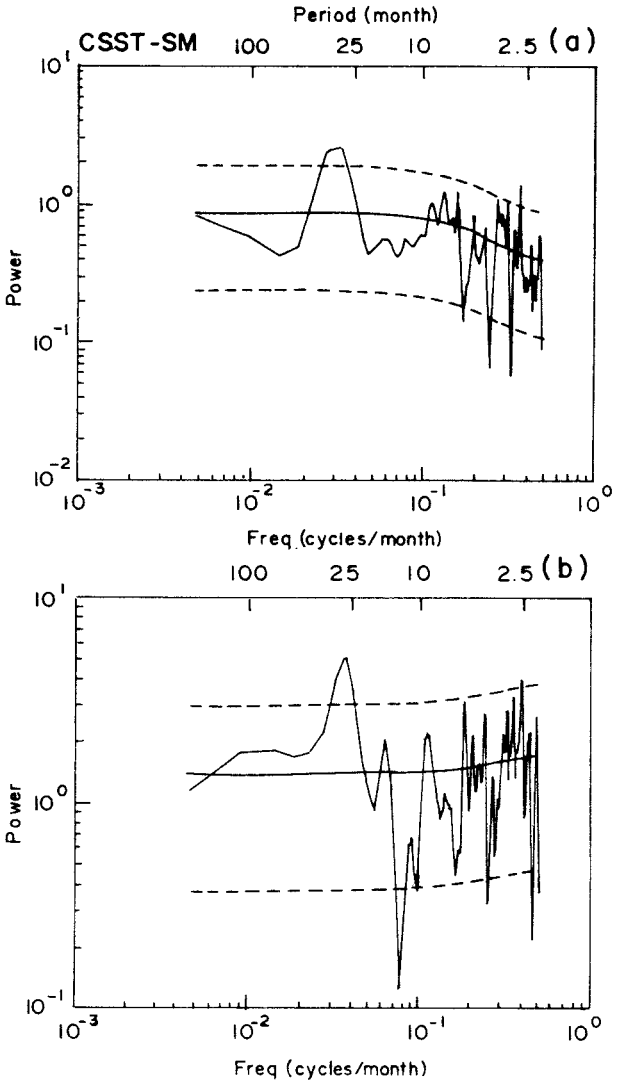

FIG. 16. Power spectra of precipitation averaged between 5°S and 5°N and over two longitudinal belts (a) (70°–95°E) and (b) (120°–140°E) from the CSST-SM simulation. Other conventions are same as in Fig. 15.

interannual variations of the monsoon, a detailed discussion on the structure and origin of the biennial mode is postponed for a future study. However, in order to provide some idea about the horizontal scale and temporal evolution of this mode, we show time–longitude sections of biennial filtered 860-mb zonal wind averaged between 5°S and 5°N for the OBS-SST run as well as the CLI-SST and CSST-SM runs in Fig. 17. The nature of the biennial signal simulated by our model in the OBS-SST run (Fig. 17a) is very similar to the observed biennial signal in the surface winds [see Fig. 10 of Ropelewski et al. (1992)]. Like the biennial component of the observed surface winds, the simulated biennial oscillation of the 860-mb wind is mostly stationary with a dipole of anomalies around 140°E but shows occasional eastward propagation as during 1981–83. The amplitude of the simulated biennial mode in the 860-mb zonal wind is slightly larger that in the observed biennial mode in surface winds as may be expected. The biennial signal in both the CLI-SST and CSST-SM runs have more or less the same amplitude, which is about one-half that in the OBS-SST run. The larger signal in the OBS-SST run is understandable as the SST boundary forcing has a clear biennial signal. Thus, in the OBS-SST run, in addition to a possible internal biennial oscillation there is an external biennial forcing. The biennial signals in the CLI-SST and in the CSST-SM runs show mainly stationary evolution. As in the OBS-SST run, the biennial oscillation in the CLI-SST and CSST-SM runs also have regional-scale dipole structures. However, the centers of the dipoles are around 90° and 120°E, respectively.

6. Summary of results and implications for monsoon predictability

The interannual variability of the Indian summer monsoon simulated by three multiyear simulations with the GFDL R30L14 model is studied. The monsoon climatology of the model is realistic, including the position and strength of the low-level westerly jet, upper-level easterly jet, and precipitation over continental India. The simulation of the onset and retreat of the monsoon precipitation is also reasonable. The simulation of the interannual variability of the planetary-scale part of the monsoon is realistic in the OBS-SST run. The simulated interannual variability of the monsoon shear index and its teleconnection with SST over both Indian and Pacific Oceans resembles the observations. As is characteristic of most AGCMs (Sperber and Palmer 1996), the skill of the model in simulating the precipitation over the Indian monsoon region is rather modest. The model is successful in simulating the precipitation differences between 1988 and 1987 over the Indian continent both in location and magnitude, but, the precipitation anomalies during 1982 and 1983 El Niño/La Niña events are not well simulated over the Indian region.

The physical mechanism linking the ENSO SST to interannual variability is further explored using a multivariate EOF analysis on several simulated fields. The analysis enables us to separate the planetary-scale response associated with the ENSO-related SST variations from other regional-scale variations and from noise. It is found that the first two modes represent the response to ENSO-related SST variations with an approximate period of around 4–5 yr, whereas the next four modes (EOF3–EOF6) represent some regional-scale modes with higher-frequency variations. A close examination of the ENSO mode reveals that this mode is associated with enhanced precipitation over the equatorial Indian Ocean and decreased precipitation over continental India. This is due to the fact that the eastward migration of the ascending branch of the Walker circulation from its normal position over Indonesia to the central Pacific

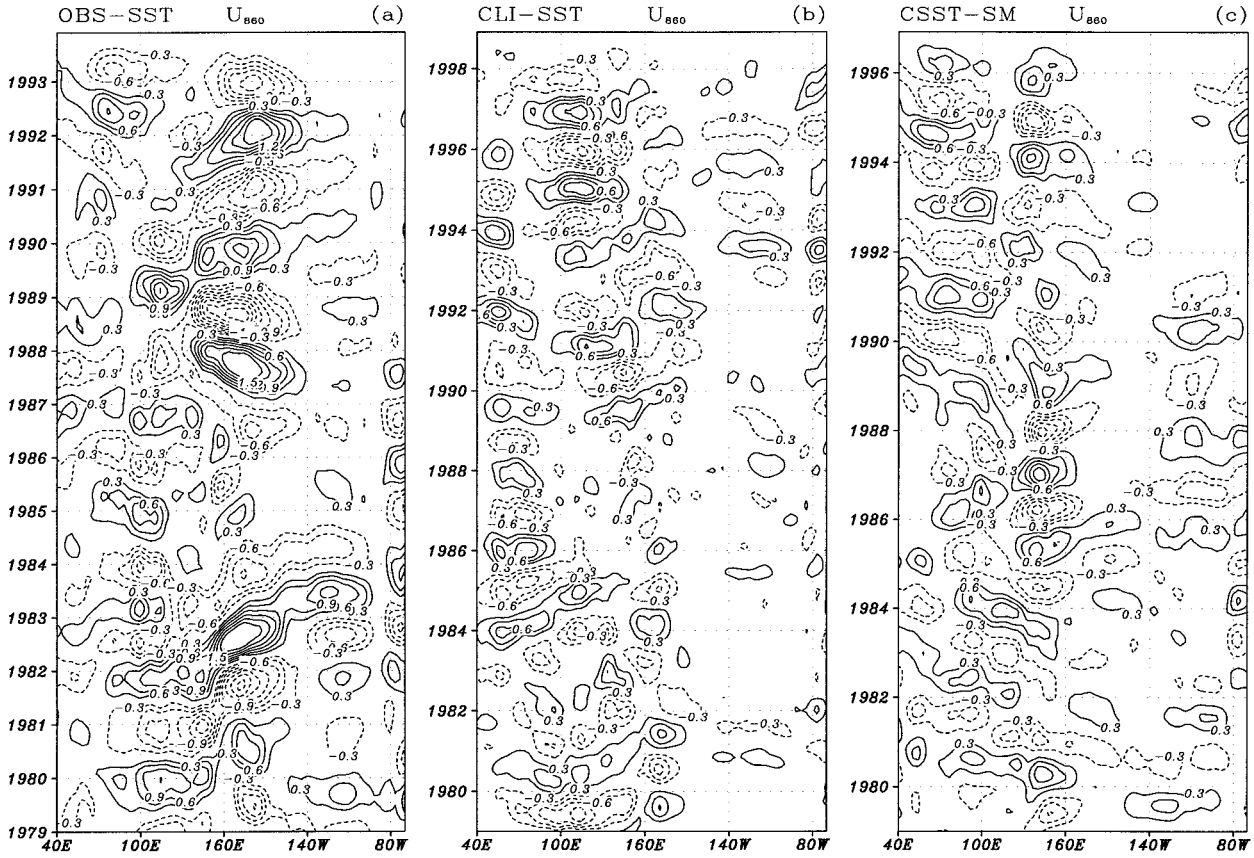

FIG. 17. Time-longitude section of biennial filtered zonal winds at 860 mb averaged around an equatorial belt (5°S–5°N). Note that (a) the OBS-SST run is for 15 yr while the (b) CLI-SST run is for 20 yr and (c) CSST-SM run is for 18 yr. Negative contours interval are dotted and units are in m s^{-1}. Uniform contour interval of 0.3 m s^{-1} is used and the zero contour is not plotted.

leads to a low-level convergence anomaly over the equatorial Indian Ocean. This change in the large-scale circulation favors the equatorial ITCZ leading to enhanced precipitation over this region. A favorable equatorial ITCZ leads to suppression of the continental one through subsidence over continental region associated with it. It is shown that over the continental region the contribution of the regional modes may be even larger than that of the ENSO modes. While the ENSO mode may be more predictable due to forcing essentially coming from slow SST variation, it is conjectured that the predictability of the regional modes may be much lower. This is because the regional modes do not seem to be forced by large-scale variations of SST. We suspect that some of these regional modes may arise due to internal dynamics.

The above conjecture is further supported by examination of the interannual variability of several summer monsoon indexes from the CLI-SST run. The simulated interannual variations of several monsoon indexes in this run are comparable in magnitude but somewhat weaker than those simulated in the OBS-SST run. It is further demonstrated that the interannual variability in the CLI-SST run is due to a significant biennial oscillation of the model atmosphere. The CSST-SM experiment was carried out to address whether the biennial oscillation could have resulted from a soil moisture–atmosphere feedback or whether it was internal to the atmosphere. The fact that a significant biennial oscillation is seen even in the fixed soil moisture run establishes that the biennial oscillation is an internal mode of the model atmosphere. Interaction between atmospheric high-frequency transients (synoptic and intraseasonal oscillations) and the annual cycle is proposed as a candidate for the biennial oscillation in our model atmosphere (Goswami 1995).

The biennial internal oscillation is likely to be a major limiting factor for prediction of seasonal monsoon precipitation. The biennial mode has largest amplitude around the precipitating zone over the Indonesian region. As the ENSO response is relatively weak over the Indian region, and the biennial internal mode has large amplitude over this region, it may dominate the interannual variability. Although the amplitude of the biennial mode is large over northern Australia, the ENSO response is also large over this region. As a result the biennial mode cannot dominate the interannual variability over northern Australia. Over the Sahel region

in Africa the amplitude of the biennial oscillation is very weak. Therefore, the interannual variations over the Sahel are again primarily governed by SST variations. These conclusions from our analysis are consistent with conclusions that the seasonal predictions of precipitation over the Sahel (Palmer and Anderson 1994; Rowell et al. 1995) and northern Australia based on SST can be made with much greater confidence than can be done over the Indian monsoon region (Brankovic and Palmer 1994). Thus, in conclusion, we can say that the Charney and Shukla (1981) hypothesis may still be applicable over most of the Tropics. However, we should recognize that the monsoon region is unique in the Tropics, has limited predictability, and must be treated differently.

It may be noted here that, in a recent study, Alexander and Weickmann (1995) examined the simulated biennial variability in a R15L9 version of GFDL's climate model. They compared a 35-yr simulation with observed SST from January 1950 to December 1984 with a similar 35-yr control run with climatological SST. They find that the observed SST run simulates a biennial signal in near-surface winds with one-half to two-thirds the observed amplitude. The climatological SST run also simulates a biennial signal but it is weaker and does not seem to be statistically significant. On this basis, they conclude that strong oceanic forcing is essential for the observed tropical biennial variability. We show that the higher-resolution (R30L14) version of the same model with improved physics is capable of simulating a significant internal biennial variability. Therefore, strong air–sea interaction may not be essential for the observed biennial oscillations. It may be noted that while the R30 version of the model is capable of simulating the observed tropical 30–50-day intraseasonal oscillations (Hayashi and Golder 1993), the low-resolution model does not simulate them. The existence of a biennial oscillation in the R30 model and the lack of it in the R15 model is consistent with our hypothesis that the biennial oscillation arises as a result of an interaction of the intraseasonal oscillations with the seasonal cycle. The differences in the results of these two models, however, brings up the question of model dependency of the current results, which is a topic for future study.

Acknowledgments. I am indebted to Suki Manabe without whose time, help, and encouragement this work could not have been completed. He made the results of the already existing CLI-SST experiment with the same model available to me and helped in extending the OBS-SST run for the latest 5 yr. He also got the new CSST-SM run conducted for this study. A number of insightful discussions with him helped me design the experiments. His careful reading of an earlier version of the manuscript and the detailed suggestions made by him led to a much improved manuscript. I am thankful to Dick Wetherald, Mike Spellmann, Gabriel Lau, and Steve Griffies for many useful discussions. I also thank Mike Fennessy and Sumant Nigam for suggestions on an earlier version of the manuscript. I am also grateful to Kirk Bryan, Jerry Mahlman, and George Philander for their warm hospitality. Constructive comments by two anonymous reviewers helped to improve the revised manuscript. I would also like to thank K. Rajendran, H. Annamalai, and N. H. Saji for various help in analyzing the output of the model.

APPENDIX

A Brief Description of the Physical Parameterizations in the GFDL R30L14 Climate Model

Precipitation is computed following the ''moist convective adjustment scheme'' described by Manabe et al. (1965). Distinction is made between rainfall and snowfall depending on whether the temperature above the surface is above or below freezing, respectively. Soil moisture is computed by the so-called bucket method (Manabe 1969). Within the model, the soil is assumed to have the ability to contain 15 cm of liquid water. Over the continents, surface temperature is computed from the condition of heat balance at the surface assuming a zero heat capacity. The scheme for computation of albedos of snow cover and sea ice is described by Manabe et al. (1991). For snow-free land or ice-free ocean, the surface albedo is prescribed geographically based on a study by Posey and Clapp (1964). The model also includes a gravity wave drag formulation developed by Y. Hayashi and described by Broccoli and Manabe (1992). A simple mixing length theory for vertical diffusion of momentum, heat, and moisture is also included.

Prediction of cloud cover is done following the scheme used by Wetherald and Manabe (1988) with the following modifications. 1) Overcast cloud is placed whenever the relative humidity is equal to or exceeds a critical value. The critical value varies as a linear function of atmospheric pressure from 100% at the surface to 90% at the top of the model atmosphere. 2) Cloud reflectivity and absorptivity for solar radiation are prescribed separately for high, middle, and low clouds as a function of the zenith angle. 3) Thick clouds (clouds occupying more than one finite-difference level) are assigned the same optical properties as thin clouds depending upon in which height category the cloud base occurs. 4) The height classification of high, middle, and low clouds are prescribed as functions of latitude. This is to account for the lowering of the tropopause height with increasing latitude. Except high clouds, which are assigned a blackness of 60%, all clouds are assumed to be blackbodies. These modifications made it possible to remove almost all annual mean global radiation imbalance at the top of the model atmosphere based upon observed sea surface temperature and sea ice.

REFERENCES

Alexander, M. A., and K. M. Weickmann, 1995: Biennial variability in an atmospheric general circulation model. *J. Climate,* **8,** 431–440.

Brankovic, C., and T. Palmer, 1994: Predictability of summer monsoon. *Proc. Int. Conf. On Monsoon Variability and Prediction,* Trieste, Italy, WMO, 629–636.

——, ——, and L. Ferranti, 1994: Predictability of seasonal atmospheric variations. *J. Climate,* **7,** 217–237.

Broccoli, A. J., and S. Manabe, 1992: The effects of orography on midlatitude Northern Hemisphere dry climates. *J. Climate,* **5,** 1181–1201.

Charney, J. G., and J. Shukla, 1981: Predictability of monsoons. *Monsoon Dynamics,* J. Lighthill and R. P. Pearce, Eds., Cambridge University Press, 99–109.

Chen, T.-C., and M.-C. Yen, 1994: Interannual variation of the Indian monsoon simulated by the NCAR Community Climate Model: Effect of the tropical Pacific SST. *J. Climate,* **8,** 1403–1415.

Delworth, T., S. Manabe, and R. J. Stouffer, 1993: Interdecadal variations of the thermohaline circulation in a coupled ocean–atmosphere model. *J. Climate,* **6,** 1993–2011.

Dickson, R. R., 1984: Eurasian snow cover versus Indian monsoon rainfall—An extension of Hahn-Shukla results. *J. Climate Appl. Meteor.,* **23,** 171–173.

Dumenil, L., K. Arpe, and L. Bengtsson, 1994: Variability of the Indian monsoon in the ECHAM3 model. Part I: MONEG and AMIP experiments. *Proc. Int. Conf. on Monsoon Variability and Prediction,* Trieste, Italy, WMO, 609–620.

Fennessy, M., and J. Shukla, 1994: Simulation and predictability of monsoons. *Proc. Int. Conf. on Monsoon Variability and Prediction,* Trieste, Italy, WMO, 567–575.

Gadgil, S., 1988: Recent advances in monsoon research with particular reference to Indian monsoon. *Aust. Meteor. Mag.,* **36,** 193–204.

Gordon, C. T., and W. Stern, 1982: A description of the GFDL global spectral model. *Mon. Wea. Rev.,* **110,** 625–644.

Goswami, B. N., 1994: Dynamical predictability of monsoons—Problems and prospects. *Proc. Indian Natl. Sci. Acad.,* **61A,** 101–120.

——, 1995: A multiscale interaction model for the origin of the tropospheric QBO. *J. Climate,* **8,** 524–534.

——, J. Shukla, E. K. Schneider, and Y. C. Sud, 1984: Study of the dynamics of the intertropical convergence zone with a symmetric version of the GLAS climate model. *J. Atmos. Sci.,* **41,** 5–19.

——, V. Krishnamurthy, and N. H. Saji, 1995: Simulation of ENSO related surface winds in the tropical Pacific by an atmospheric general circulation model forced by observed sea surface temperature. *Mon. Wea. Rev.,* **123,** 1677–1694.

Hahn, D. J., and J. Shukla, 1976: An apparent relationship between Eurasian snow cover and Indian monsoon rainfall. *J. Atmos. Sci.,* **33,** 2461–2462.

Harzallah, A., and R. Sadourny, 1995: Internal versus SST-forced atmospheric variability simulated by an atmospheric general circulation model. *J. Climate,* **8,** 474–495.

Hayashi, Y., and D. G. Golder, 1993: Tropical 40–50 and 20–30 day oscillations appearing in realistic and idealized GFDL climate models. *J. Atmos. Sci.,* **50,** 464–494.

Kitoh, A., 1991: Interannual variations in an atmospheric GCM forced by the 1970–1989 SST. Part I: Response of the tropical atmosphere. *J. Meteor. Soc. Japan,* **69,** 251–269.

Latif, M., J. Biercamp, H. von Storch, M. McPhaden, and E. Kirk, 1990: Simulation of ENSO related surface wind anomalies with an atmospheric GCM forced by observed SST. *J. Climate,* **3,** 509–521.

Lau, N. C., 1985: Modelling the seasonal dependence of atmospheric response to observed El Niño in 1962–1976. *Mon. Wea. Rev.,* **113,** 1970–1996.

Legates, D. R., and C. J. Willmott, 1990: Mean seasonal and spatial variability in gauge-corrected global precipitation. *Int. J. Climatol.,* **10,** 111–127.

Levitus, C., 1982: *Climatological Atlas of the World Ocean.* National Oceanic and Atmospheric Administration, 163 pp.

Manabe, S., 1969: Climate and the ocean circulation. Part 1: The atmospheric circulation and hydrology of the earth's surface. *Mon. Wea. Rev.,* **97,** 739–744.

——, and R. J. Stouffer, 1994: Multiple-century response of a coupled ocean–atmosphere model to an increase of atmospheric carbon dioxide. *J. Climate,* **7,** 5–23.

——, J. Smagorinsky, and R. F. Strickler, 1965: Simulated climatology of a general circulation model with a hydrologic cycle. *Mon. Wea. Rev.,* **93,** 769–798.

——, R. J. Stouffer, M. S. Spellman, and K. Bryan, 1991: Transient response of a coupled ocean–atmosphere model to gradual changes of atmospheric CO_2. Part I: Annual mean response. *J. Climate,* **4,** 785–818.

Meehl, G. A., 1987: The annual cycle and interannual variability in the tropical Indian and Pacific Ocean regions. *Mon. Wea. Rev.,* **115,** 27–50.

——, 1993: A coupled air–sea biennial mechanism in the tropical Indian and Pacific regions: Role of the ocean. *J. Climate,* **6,** 31–41.

——, 1994: Coupled land-ocean-atmosphere processes and the biennial mechanism in the south Asian monsoon region. *Proc. Int. Conf. on Monsoon Variability and Prediction,* Trieste, Italy, WMO, 637–644.

Nigam, S., 1994: On the dynamical basis for the Asian monsoon rainfall–ENSO relationship. *J. Climate,* **7,** 1750–1771.

——, and H. S. Shen, 1993: Structure of oceanic and atmospheric low frequency variability over the tropical Pacific and Indian Oceans. Part I: COADS observations. *J. Climate,* **6,** 657–676.

North, G. R., T. L. Bell, R. F. Cahalan, and F. J. Moeng, 1982: Sampling errors in the estimation of empirical orthogonal functions. *Mon. Wea. Rev.,* **110,** 699–706.

Palmer, T. N., and D. Anderson, 1994: The prospect of seasonal forecasting—A review paper. *Quart. J. Roy. Meteor. Soc.,* **120,** 755–793.

——, C. Brankovic, P. Viterbo, and M. J. Miller, 1992: Modelling interannual variations of summer monsoons. *J. Climate,* **5,** 399–417.

Posey, J. W., and P. F. Clapp, 1964: Global distribution of normal surface albedo. *Geofis. Int.,* **4,** 33–48.

Rao, Y. P., 1976: *Southwest Monsoon. Synoptic Meteorology. Meteor. Monogr.,* No. 1, India Meteorological Dept., 367 pp.

Rasmusson, E. M., and T. H. Carpenter, 1983: The relationship between eastern equatorial Pacific sea surface temperature and rainfall over India and Sri Lanka. *Mon. Wea. Rev.,* **111,** 517–528.

Reynolds, R., 1988: A real time global sea surface temperature analysis. *J. Climate,* **1,** 75–86.

Ropelewski, C. F., M. S. Halpert, and X. Wang, 1992: Observed tropospheric biennial variability and its relationship with Southern Oscillation. *J. Climate,* **5,** 594–614.

Rowell, D., C. K. Folland, K. Maskell, and M. N. Ward, 1995: Variability of summer rainfall over tropical north Africa (1906–1992): Observations and modelling. *Quart. J. Roy. Meteor. Soc.,* **121,** 669–704.

Shukla, J., 1981: Dynamical predictability of monthly means. *J. Atmos. Sci.,* **38,** 2547–2572.

——, and Y. Mintz, 1982: Influence of land-surface evapotranspiration on the earth's climate. *Science,* **214,** 1498–1501.

——, and D. A. Paolino, 1983: The Southern Oscillation and long range prediction of summer monsoon rainfall over India. *Mon. Wea. Rev.,* **111,** 1830–1837.

Sikka, D. R., and S. Gadgil, 1980: On the maximum cloud zone and the ITCZ over Indian longitude during the southwest monsoon. *Mon. Wea. Rev.,* **108,** 1840–1853.

Sperber, K., and T. N. Palmer, 1996: Interannual tropical rainfall variability in general circulation model simulations associated

with the Atmospheric Model Intercomparison Project. *J. Climate*, **9,** 2727–2750.
Stern, W., and K. Miyakoda, 1995: The feasibility of seasonal forecasts inferred from multiple GCM simulations. *J. Climate*, **8,** 1071–1085.
Vernekar, A. D., J. Zhou, and J. Shukla, 1995: The effect of Eurasian snow cover on Indian monsoon. *J. Climate*, **8,** 248–266.
Walsh, J. E., and C. M. Johnson, 1979: An analysis of Arctic sea ice fluctuations, 1953–1977. *J. Phys. Oceanogr.,* **9,** 580–591.
Wang, B., 1992: The vertical structure and development of the ENSO anomaly mode during 1979–1989. *J. Atmos. Sci.,* **49,** 698–712.
Webster, P. J., and S. Yang, 1992: Monsoon and ENSO: Selectively interactive systems. *Quart. J. Roy. Meteor. Soc.,* **118,** 877–926.
Wetherald, R. W., and S. Manabe, 1988: Cloud feedback processes in a general circulation model. *J. Atmos. Sci.,* **45,** 1397–1415.
Yasunari, T., 1991: The monsoon year—A new concept of the climate year in the tropics. *Bull. Amer. Meteor. Soc.,* **72,** 1331–1338.
Zwally, H. M., J. C. Comiso, C. L. Parkinson, W. J. Campbell, F. D. Carsey, and P. Gloersen, 1983: Antarctic sea ice 1973–1976: Satellite passive microwave observations. NASA SP-459. [NTIS N84-10718/4.]
Zwiers, F. W., 1993: Simulation of the Asian summer monsoon with the CCC GCM-1. *J. Climate*, **6,** 470–486.